Digest Journal of Nanomaterials and Biostructures Vol. 19, No. 4, October-December 2024, p. 1937-1946

Advanced supercapattery materials: hydrothermally synthesized niobium sulfide/reduced graphene oxide composites

W. Abbas [a,*], I. M. Moussa [b], Khalid M. Elhindi [c], C. W. Dunnill [d]
[a] *Department of Physics, COMSATS University Islamabad, Lahore Campus, Pakistan*
[b] *Department of Botany and Microbiology, College of Science, King Saud University, P.O. Box 2455, Riyadh, 11451, Saudi Arabia*
[c] *Plant Production Department, College of Food & Agriculture Sciences, King Saud University, P.O. Box 2460, Riyadh 11451, Saudi Arabia*
[d] *Energy Safety Institute (ESRI), Swansea University Bay Campus, Swansea, SA1 8EN, UK*

Supercapattery combines batteries with the advantages of supercapacitors. The hydrothermal method was employed to synthesize niobium sulfide (NbS), then doped them with reduced graphene oxide (rGO). A total surface area of 15.50 m^2/g was identified for NbS/N-GQDs by Brunauer-Emmett-Teller (BET). The composite niobium sulfide (NbS/rGO) displayed 858 Cg^{-1} regarded as a higher specific capacity (Cs) in the three-electrodes assembly. To construct an asymmetric supercapacitor, battery-graded NbS/rGO was used as the +ve as well as AC as the -ve terminals respectively. The Nbs/rGO//AC demonstrated maximum Cs of 190 Cg^{-1} besides power and energy densities of 1510 WKg^{-1} and 34.6 $WhKg^{-1}$ respectively. 90% of the initial capacity of NbS/rGO//AC remained after 5000 cycles. Future energy storage systems can use NbS/rGO as a nanostructured electrode due to its remarkable electrochemical efficiency.

(Received September 20, 2024; Accepted December 11, 2024)

Keywords: Energy Storage; Nanoparticle synthesis; Supercapacitor; Asymmetric device; rGO doping; power density; Energy density

1. Introduction

The decreasing availability of confined fossil resources has increased in this century, causing an energy crisis. To address this need, there is an increasing demand for highly efficient energy storage and transition technologies. [1-4]. Capacitors store charges electrostatically, whereas batteries store charges by faradic interactions with electrodes and electrolytes. [5, 6]. Compared to traditional chemical storage technologies, supercapacitors, frequently referred to as ultra-capacitors, have several advantages, such as a high power density and a long cyclic life. [7]. Intermediate energy and power can be produced via pseudo capacitors (PSc), which use reversible diffusion-controlled mechanisms to store electrical energy at the boundary of electrode materials. [8]. Two essential components that allow S.C.s to regulate the energy density include cell potential as well as electrode capacitance. [9]. Designing a nanoscale, porous electrode material having higher energy density values is one way to boost capacitance. Constructing asymmetric or hybrid energy storage devices, which raise the cell's overall potential, is a further strategy. Two forms of asymmetric/hybrid S.C.s are further classified. Two capacitive electrodes are used in the first kind of hybrid devices, such as EDLCs and PCs. Two forms of asymmetric/hybrid S.C.s have also been distinguished. The first class of hybrid devices with two capacitive electrodes includes PCs as well as EDLCs. Individual capacitive electrodes have been combined alongside a battery-graded electrode in the second kind of hybrid device. [10, 11]. That kind of hybrid device is known to be a supercapattery [12]. Because of their beneficial electrical and conductive qualities, metal sulfides, oxides, and particularly

* Corresponding author: waseemabbas9883@gmail.com
https://doi.org/10.15251/DJNB.2024.194.1937

phosphates/phosphides, are often used as active materials in electrode design. They can also be used in charge-storage devices because of these qualities.

Niobium sulfide (NbS) has gained popularity to be an anode material due to its extended cycle life, increased specific capacity, as well as better electrical conductivity. [13]. The application of niobium-oxide to enhance the hybrid capacitor was explored by Liao *et al*. Still, much more effort is needed to develop niobium-base materials for SC electrodes. [14]. The SCs can greatly benefit from the usage of materials based on nickel. On the other hand, combining niobium with two metals can effectively boost its conductivity. Excellent electrical conductivity, flexibility, hardness, extended cyclic retention, remarkable electrochemical characteristics, and high energy storage capacity distinguish NbS. [15].

Organic Graphene quantum dots have impressive interval-to-diameter ratios and higher surface area, along with other chemical and physical characteristics. [16]. A variety of methods for decreasing chemicals are often used in GO reduction (rGO) agents. [17, 18]. Recent developments in energy storage systems have used 2D materials like graphene, MXenes, MoS_2, etc. to improve the EES device's performance. Each type of material's GO nanosheets, with their flawless 2D carbon structure, showed unmistakably better electrochemical properties. Its impressive mechanical strength, and excellent electrical conductivity, with unusually large electrolyte achievable surface area are the reasons for this. However, during composite manufacturing, graphene undergoes significant agglomeration, which lowers the specific active area available for electrolyte interaction. This limit harms its specific capacitance along with energy density. Adding the right catalytic material into the host composite electrode materials is a workable way to solve the graphene (GO) restocking problem and improve the redox active reactions on the surface of the active composite electrode materials. [19].

In this work, niobium sulfide was doped with nitrogen-graphene quantum dots (N-GQDs) using the hydrothermal method. Scanning electron microscopy (SEM) was employed to examine morphology. X-ray diffraction (XRD) has been used to investigate NbS/N-GQDs structural properties. The material structure was examined using the X-ray photoelectron spectrum (XPS). Mostly researchers focused on replacing battery-grade electrodes in previous investigations. We adjust combined capacitive as well as battery-graded electrodes during this work. NbS/N-GQDs was used as the +ve terminal and AC was used as the -ve terminal for preparing an asymmetric device. Cyclic voltammetry (CV), galvanometric charge-discharge (GCD), specific capacity (Cs), electrochemical impedance spectroscopy (EIS), and stability testing were used in the electrochemical testing of NbS/N-GQDs.

2. Experimental section

2.1. Materials

We purchased activated carbon (AC) and KOH pellets. Niobium nitrate ($NbNO_3$), carbon black (CB), PVDF, NMP, and sodium sulfide hydrate ($Na_2S.nH_2O$) from Sigma Aldrich are also included. The nickel foam was acquired with the assistance of Urich Technology Malaysia. Every chemical was acquired through a commercial purchase and used before any kind of purification. Purchased from ALS Co. LTD. in Japan, the Pt wire and Hg/HgO were utilized as reference and counter electrodes, respectively.

2.1.1. Synthesis of Niobium sulfide

A hydrothermal method was used for making niobium sulfide. The hydrothermal process was adopted as the method of synthesis since it was straightforward and effective. Moreover, it offers more crystallinity than alternative methods like the co-precipitation process. [21]. During the hydrothermal method, the ideal temperature limit is 120–250 °C. The 30ml of deionized water (DIW) was used to create 0.8 mol solutions of sodium sulfide hydrate ($Na_2S.9H_2O$) and niobium nitrate hex hydrate ($NbH_{12}NO_9$). Subsequently, we agitated the hex hydrate niobium nitrate ($NbH_{12}NO_9$) solution continuously for 30 minutes while adding drops of $Na_2S.9H_2O$. Subsequently, the resultant solution was autoclaved for six hours at 120 °C. To remove impurities, this synthetic

material was repeatedly cleaned with water and ethanol. After being dehydrated in an oven for four hours at 50 °C, the material was then obtained.

3. Results and discussion

The materials are examined using X-ray diffraction to confirm that they are crystalline. Figure 1(a) displays the X-ray diffraction peaks of NbS/rGO. The XRD peaks observed at 2θ = 15.2°, 29.6°, 53.8°, and 64.5°, which correspond to (002), (100), (110), and (200), represent the NbS contribution. Conversely, the rGO XRD peaks, which correlate to (001), (002), and (111), were found at 2θ = 10.6°, 25.4° and 45.5°. These XRD peaks in composite conditions validate the synthesis of NbS/rGO.

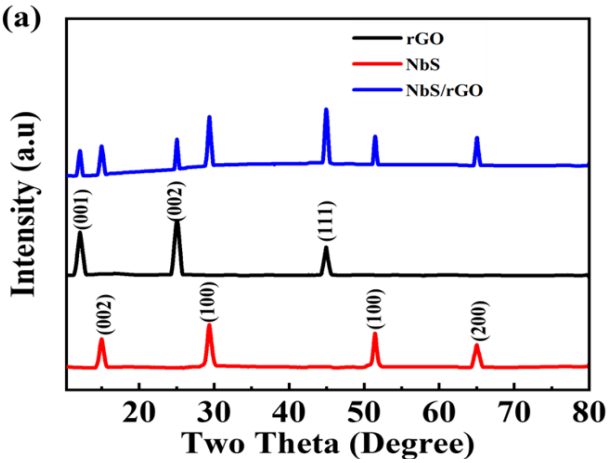

Fig. 1. (a) XRD of NbS, rGO, and NbS/rGO composite.

Table 1. The evaluation of energy density versus power density of earlier researches in the field.

Compound name	Power density	Energy Density	Specific Capacity	Reference.
ZnS/MnS	7.78	91		[29]
Co-MOF/polyaniline	1600	23.2	162.5	[30]
NbS/rGO	**Supercapattary**		**858**	**This Work**

3.1. Measurement of NbS/rGO electrodes electrochemically

NbS doped NbS/rGO electrochemical characteristics are studied by analyzing cyclic voltammetry (CV), and galvanostatic charge-discharge (GCD). The CVs of all three samples were evaluated at various scan rates from 3 to 50 mVs^{-1}, all within the 0 to 0.8 V potential range. Figure 2(a–b) displays the CV graphs for NbS and NbS/rGO, respectively. The redox peaks on the graph shapes show NbS/rGO. Faradaic performance is an indication of battery-type materials. When the OH-ions of the electrolyte come in contact with the working electrode, the faradaic reaction takes place. As the scan rate rises, oxidation/reduction peaks display increasing current values. The Cs of electrodes were determined using the given formula.

$$Q_s = \frac{1}{mv}\int_{V_i}^{V_f} I \times VdV \quad (1)$$

The variable Q_s in the calculation given stands for specific capacity, $\int_{V_i}^{V_f} I \times VdV$represents the CV curve's area, whereas the m and v stand for scan rate as well as active mass, accordingly. This formula is divided by the 0.7 V potential range "V" to find the specific capacity (Cs).

Equation (1) obtains specific capacities for NbS and NbS/rGO of 702 Cg^{-1} and 1089 Cg^{-1}. The oxidation peaks displayed an additional increase after the NbS composite was doped with rGO. [20, 21]. At this point, several attractive surface regions are dominated by the material NbS/rGO, resulting in them being unavailable for charge storage. An interesting finding about the doped material from Figure 2(a-b) is the moving of oxidation peaks to a higher potential, showing a decreased oxidation rate of rGO, even though, NbS/N-GQDs exhibit larger peaks than the NbS sample. In contrast to previous samples, the broad surface of the doped compound exhibits a more current response. When the CV performance of each sample is compared, the NbS sample outperformed the others due to its larger area over the curve and higher specific capacity. The specific capacities for NbS and NbS/rGO were found to be 703 Cg^{-1} and 1085 Cg^{-1} as displayed in Figure 2(c).

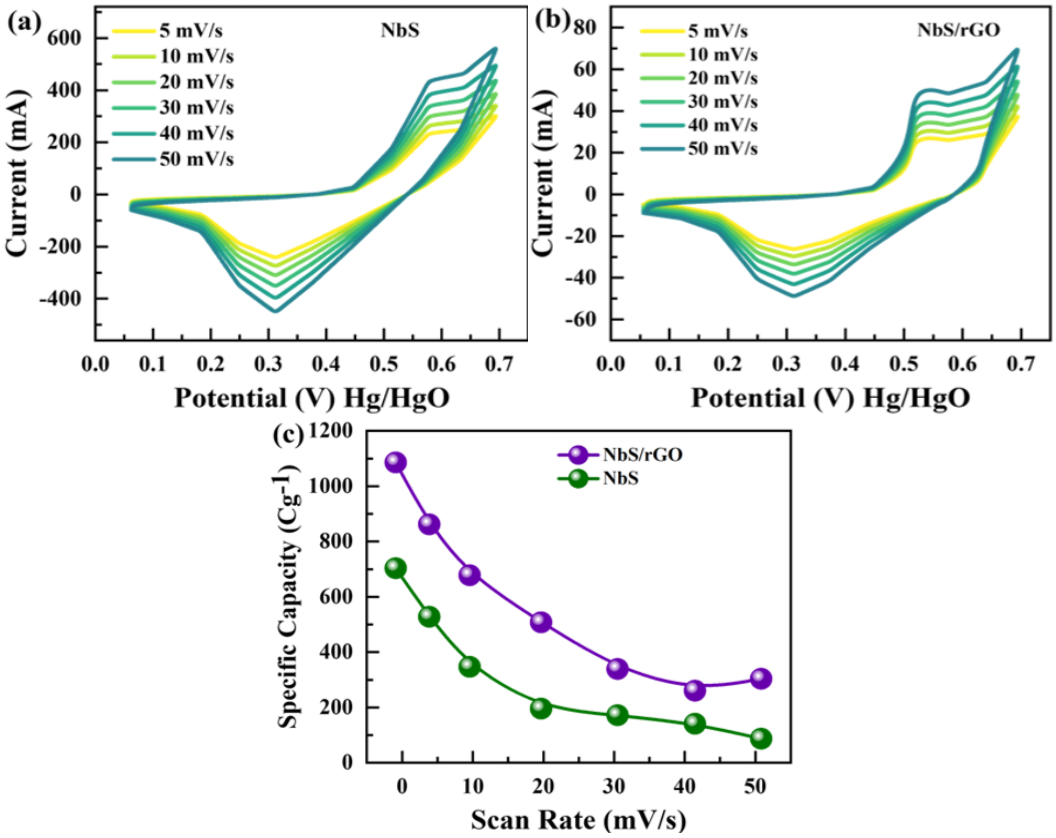

Fig. 2. Cyclic voltammetry for (a) NbS (b) NbS/rGO (c) Specific capacity of NbS and NbS/rGO at various scan rates.

Figure 3 shows the electrode analysis findings from GCD at 1 to 2.6 Ag^{-1} current density range in potential ranges of 0 to 0.60 V. This material is considered battery-grade, as shown by the non-linear behavior of galvanostatic charging and discharging in Figure 3. These figures show that the specific capacity consequently decreases the discharge time with increasing current density. The limited period that the electrolyte ions and electrode material may interact is the cause of the shorter discharge period. At greater current densities, the charge carrier interaction which is the result of increased interest causing internal resistance also contributes to the drop-in discharge time. The Cs of electrodes via GCD can be calculated by the expression given below.

$$Q_s = \frac{I \times t}{m} \quad (2)$$

where, current and discharge time are denoted by "I" and "t," respectively.

At 1 A/g, the NbS showed 594 C/g, and the NbS/rGO 858 C/g in Figure 3(c). Because of its quicker ion diffusion channel for electrolytes in contact with the material deposited on the electrode, NbS/rGO shows high specific capacity.[22, 23].

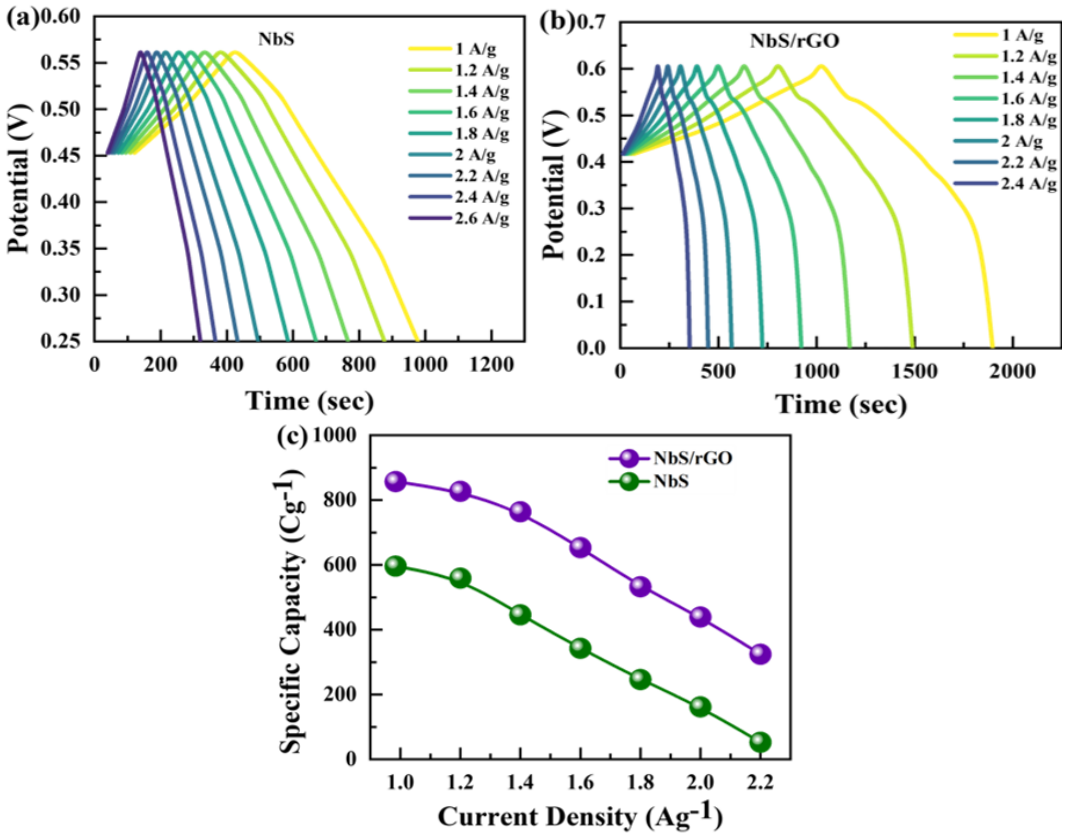

Fig. 3. (a) GCD for NbS (b) Doped material NbS/rGO GCD Curves (c) Specific capacity of NbS and NbS/rGO via GCD at different current density values.

Using the BET technique, its pore size, pore volume, and surface area were measured. BET calculates surface area and is used to measure the adsorption isotherm. Although it performs well with materials that exhibit isotherm curves, this technique is often applied to a variety of materials [21]. Here is the NbS/rGO isotherm shown in Figure 4(a). The NbS/rGO has a pore volume of 0.038 cm^3/g and a surface area of 16.69 m^2/g. Its pore size of 21.12 nm gives the appearance of rapid ion movement. These results suggest that a substantial quantity of charge may be rapidly stored in NbS/rGO due to its large pore size and high surface area. With cycle stability, this increased surface area immediately improved the specific capacity. A larger surface area facilitates stronger charge accumulations, but increased hole volume expedites ion transportation. The EIS measurement is shown in Figure 4(b).

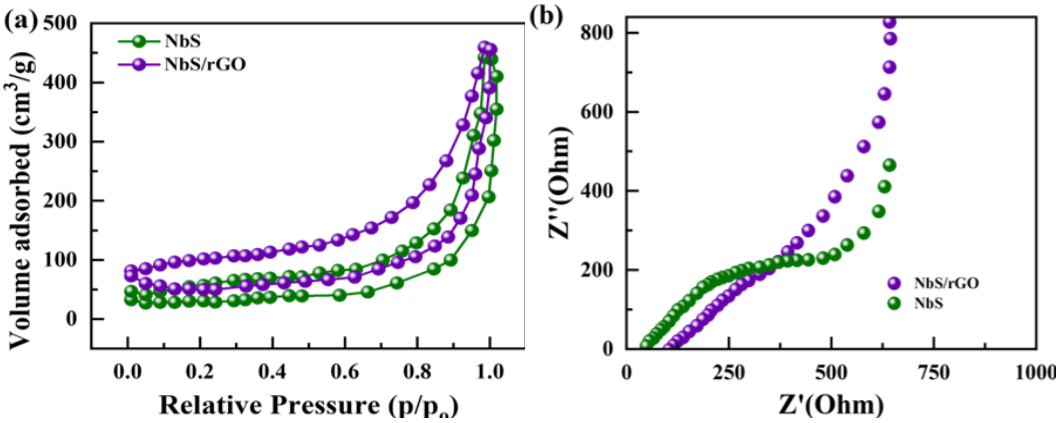

Fig. 4. (a) BET of NbS and NbS/rGO. (b) EIS of NbS and NbS/rGO.

NbS/rGO has a lower impedance, which makes it more advantageous for supercapattery design. Because the components' properties resemble those of a battery, the EIS form in this instance cannot be completely vertical. The cause of this increased conductivity is rGO.

To perform more studies on the material's efficiency, a supercapattery device is made. With the sample NbS/rGO as the +ve electrode and carbon black as the -ve electrode. To make a device that can be used in daily life, the best sample was combined with activated carbon. After a two-electrode system has been fabricated, the assessment of GCD and CV test performance at different current densities at various scan rates is shown in Figure 5(a–c). To construct the real device, the positive electrode was the binary composite material sample NbS/rGO, while the negative electrode was activated carbon. Electrochemical characterization of this device was performed in an electrolyte solution containing 1M KOH. Equation (3) below illustrates how the object's Cs and potential range are the only factors that affect the energy density.

$$E = \frac{1}{2}CV^2 \tag{3}$$

where "V" stands for a prospective window and "C" for specified capacity [24]. For sample NbS/rGO, the independent calculation of the CV peaks in a three-electrode assembly is performed at 3 mVs^{-1}, and the AC over potential is between 0 and 0.6 V and -1 to 0 V. Within 0 to 1.6 V potential range, the scan rates from 5 mVs^{-1} to 100 mVs^{-1} using the NbS/rGO electrodes and activated carbon in CV graph. The presence of redox peaks at higher potentials and non-rectangular CV curves indicates a non-capacitive, battery-graded character. The CV curves at lower potentials show capacitive behavior. The device's remarkable rate capabilities can be explained by the form retention of CV at higher scan rates. Using GCD, the device's behavior was further examined in 0 to 1.6 V potential range from 1 to 2.4 Ag^{-1} current density range.

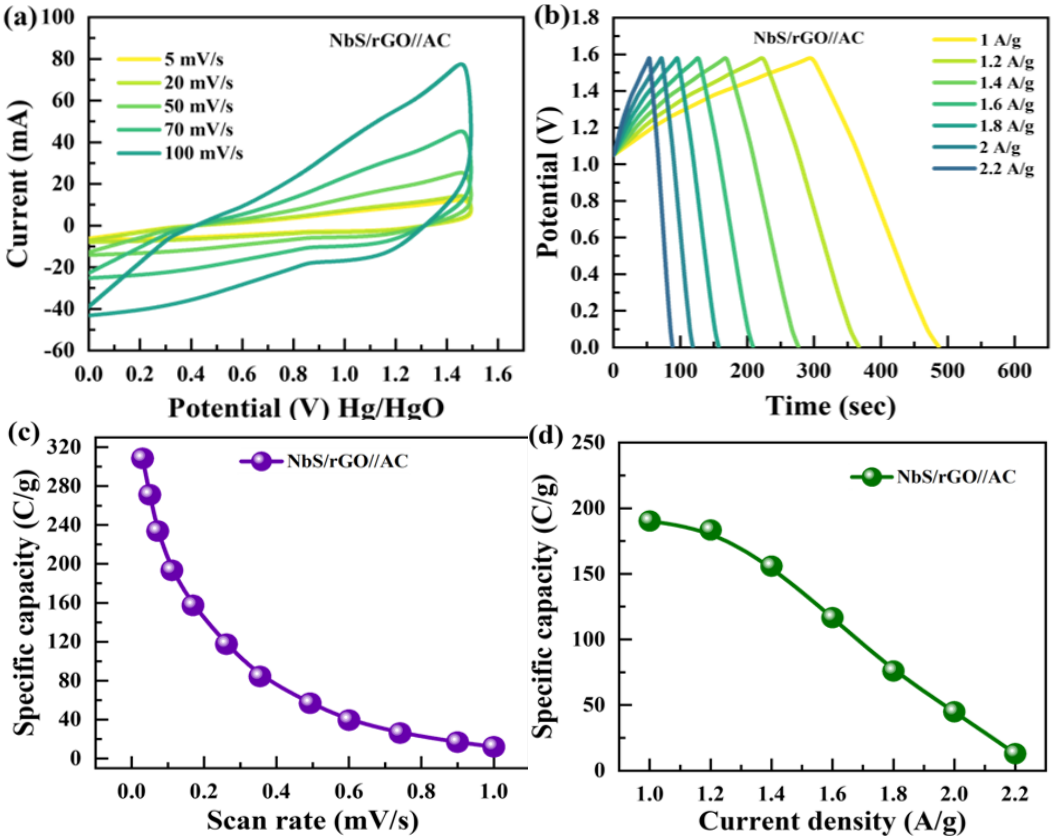

Fig. 5. (a) Two-electrodes hybrid device CV curves (3 to 50 mVs^{-1}) (c) Computation of Galvanostatic charge discharge at various values of current density. (c) The calculated specific capacity for NbS/rGO//AC vs various scan rates. (d) NbS/rGO//AC specific capacity vs different current densities.

These findings improve on the potential applications of supercapattery development. The GCD peak's consistent behavior at higher current density levels and its well-preserved shape demonstrates the device's exceptional rate capacity and stability. The highest Cs of 308 C/g for the device sample NbS/rGO/AC was obtained by CV at 3 mV/s, whereas the maximum Cs of 190 C/g was determined using GCD.

A current density of 4.8 A/g was used for 5000 GCD cycles to assess the supercapattery durability. The charge/discharge time calculated over 5000 cycles is shown in Figure 6(a). The capacity retention graph, which is displayed in Figure 6(b), was found to be 84% after 5000 cycles. Figure 6(b) displays the Coulombic efficiency (CE), which is determined using the previously indicated equation following 5000 GCD cycles. The result was found to be 90%. The Nbs/rGO/AC b-values that fall within the supercapattery b-value range are shown in Figure 6(c). Additionally, the b-values suggest that supercapattery development has been in place. The battery's b-values vary from 0 to 0.5, the supercapattery's from 0.5 to 0.8, and the supercapacitors' from 0.8 to 1.0, as shown in Figure 6(d) [25]. The energy and power densities can be determined via the following formulas.

$$E\ (Wh\ kg^{-1}) = \frac{Q_s \times \Delta V}{2 \times 3.6} \tag{4}$$

$$P\ (W\ kg^{-1}) = \frac{E \times 3600}{\Delta t} \tag{5}$$

The energy density (E) for a power density of 1510 W k/g was found to be 34.6 Wh k/g, as shown in Figure 6(d). This value is higher than previously published values of un-doped sulfides, suggesting that NbS/rGO performs better in energy storage device applications [26-28]. The power and energy density of this study are compared with earlier ones in Figure 6(d).

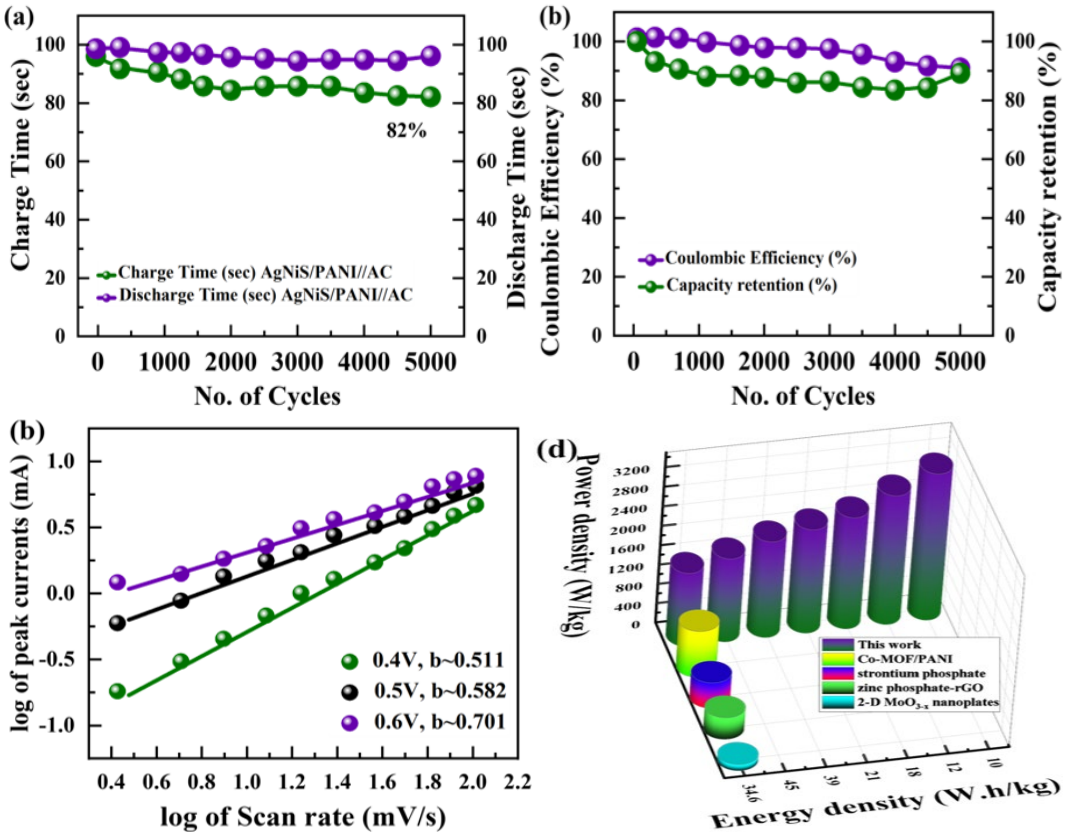

Fig. 6. (a) The device stability up to 5000 charging/discharging cycles (b) Specific capacity retention and columbic efficiency after 5000 charging/discharging cycles (c) Linear fitting for NbS/rGO//AC supercapattery (d) Comparing energy density vs power density with other's work.

Based on the improved performance of the NbS/rGO sample, it was concluded that doping with rGO enhanced the binary metal sulfide performance, making NbS/rGO an acceptable substitute for supercapattery applications.

4. Conclusion

The hydrothermal process was used in this work to produce NbS. Following the binary composite NbS/rGO, many samples are used to compare its electrochemical performance. Because of the rGO's large surface area, which promotes a longer and stronger ion diffusion channel, the NbS/rGO showed better capacity. Our supercapattery device achieved a Cs of 190 Cg^{-1} at 1 Ag^{-1} and 90% cyclic retention even after 5000 charge-discharge cycles. The device was found to have a power density of 1510 WKg^{-1} and an energy density of 34.6 $WhKg^{-1}$. These results imply that NbS/rGO may be used to develop supercapattery devices with excellent performance.

Funding

Researchers Supporting Project number (RSPD2024R952), King Saud University.

Acknowledgements

The authors extend their deep appreciation to Researchers Supporting Project number (RSPD2024R952), King Saud University, Riyadh, Saudi Arabia.

.

References

[1] Pant, B., G.P. Ojha, M.J.J.o.E.S. Park, One-pot synthesis, characterization, and electrochemical studies of tin-nickel sulfide hybrid structures on nickel foam for supercapacitor applications. 2020. 32: p. 101954; https://doi.org/10.1016/j.est.2020.101954

[2] Pant, B., et al., Carbon nanofibers wrapped with zinc oxide nano-flakes as promising electrode material for supercapacitors. 2018. 522: p. 40-47; https://doi.org/10.1016/j.jcis.2018.03.055

[3] Soudous, R., Telia, A., Meziani, A., Nasri, N., Semra, L., Experimental and ab-initio analysis of structural, electronic and optical properties of ZMCO thin films elaborated by sol-gel method for optoelectronic application, 2024. 19(4): p. 1419-1433; DOI: 10.15251/DJNB.2024.194.1419

[4] Xu, Y., et al., Preparation of SnS2/g-C3N4 composite as the electrode material for Supercapacitor. 2019. 806: p. 343-349; https://doi.org/10.1016/j.jallcom.2019.07.130

[5] Tasnin, W., L.C.J.I.R.P.G. Saikia, Performance comparison of several energy storage devices in deregulated AGC of a multi-area system incorporating geothermal power plant. 2018. 12(7): p. 761-772; https://doi.org/10.1049/iet-rpg.2017.0582

[6] Zhu, S., et al., Molten-salt directed mesopore engineering of carbon nanotubes for energetic quasi-solid-state supercapacitors. 2022. 200: p. 75-83; https://doi.org/10.1016/j.carbon.2022.08.030

[7] Zhu, S., et al., Carbon, 2022. 200: p. 75-83; https://doi.org/10.1016/j.carbon.2022.08.030

[8] Zhu, S., et al., Jahn-Teller effect directed bandgap tuning of birnessite for pseudocapacitive application. 2023. 6(3): p. e12382; https://doi.org/10.1002/eem2.12382

[9] Hassan, H.u., et al., Highly stable binary composite of nickel silver sulfide (NiAg2S) synthesized using the hydrothermal approach for high-performance supercapattery applications. 2022. 46(8): p. 11346-11358; https://doi.org/10.1002/er.7932

[10] Wu, S., Y.J.S.C.M. Zhu, Highly densified carbon electrode materials towards practical supercapacitor devices. 2017. 60(1): p. 25-38; https://doi.org/10.1007/s40843-016-5109-4

[11] Zhang, J., X.J.C. Zhao, On the configuration of supercapacitors for maximizing electrochemical performance. 2012. 5(5): p. 818-841; https://doi.org/10.1002/cssc.201100571

[12] Dubal, D.P., et al., Towards flexible solid-state supercapacitors for smart and wearable electronics. 2018. 47(6): p. 2065-2129; https://doi.org/10.1039/C7CS00505A

[13] Subha, S., et al., Characterization and antibacterial studies of Sn doped CuO nanocomposite using centratherum punctatum leaf extract. 2024. 19(2): p. 619-628; DOI: 10.15251/DJNB.2024.192.619

[14] Li, W., et al., Colloidal synthesis of NbS2 nanosheets: from large-area ultrathin nanosheets to hierarchical structures. 2020. 8: p. 189; https://doi.org/10.3389/fchem.2020.00189

[15] Danot, M., et al., Catalytic properties of niobium sulphides in the conversion of nitrogen containing molecules. 1991. 10(4): p. 629-643; https://doi.org/10.1016/0920-5861(91)80043-9

[16] Shen, J., et al., Graphene quantum dots: emergent nanolights for bioimaging, sensors, catalysis and photovoltaic devices. 2012. 48(31): p. 3686-3699; https://doi.org/10.1039/c2cc00110a

[17] McAllister, M.J., et al., Single sheet functionalized graphene by oxidation and thermal expansion of graphite. 2007. 19(18): p. 4396-4404; https://doi.org/10.1021/cm0630800

[18] Stankovich, S., et al., Synthesis of graphene-based nanosheets via chemical reduction of exfoliated graphite oxide. 2007. 45(7): p. 1558-1565; https://doi.org/10.1016/j.carbon.2007.02.034

[19] Roman, M., et al., Electrochimica Acta, 2021. 400: p. 139489; https://doi.org/10.1016/j.electacta.2021.139489

[20] Shaddad, M.N., et al., Cooperative Catalytic Effect of ZrO2 and α-Fe2O3 Nanoparticles on BiVO4 Photoanodes for Enhanced Photoelectrochemical Water Splitting. 2016. 9(19): p. 2779-2783; https://doi.org/10.1002/cssc.201600890

[21] Liang, C., et al., Synthesis of morphology-controlled silver nanostructures by electrodeposition. 2010. 2(1): p. 6-10; https://doi.org/10.1007/BF03353609

[22] Chen, X., et al., Electrochromic fiber-shaped supercapacitors. 2014. 26(48): p. 8126-8132; https://doi.org/10.1002/adma.201403243

[23] Lei, W., et al., Tungsten disulfide: synthesis and applications in electrochemical energy storage and conversion. 2020. 2(3): p. 217-239; https://doi.org/10.1007/s42864-020-00054-6

[24] Afzal, A.M., et al., ACS Applied Materials & Interfaces, 2020. 12(17): p. 19625-19634; https://doi.org/10.1021/acsami.9b22898

[25] Iqbal, M.Z., et al., Co-MOF/polyaniline-based electrode material for high performance supercapattery devices. 2020. 346: p. 136039; https://doi.org/10.1016/j.electacta.2020.136039

[26] Hassan, H.u., et al., Highly stable binary composite of nickel silver sulfide (NiAg2S) synthesized using the hydrothermal approach for high-performance supercapattery applications.

[27] Wan, H., et al., Hydrothermal synthesis of cobalt sulfide nanotubes: the size control and its application in supercapacitors. 2013. 243: p. 396-402; https://doi.org/10.1016/j.jpowsour.2013.06.027

[28] Javed, M.S., et al., High performance solid state flexible supercapacitor based on molybdenum sulfide hierarchical nanospheres. 2015. 285: p. 63-69; https://doi.org/10.1016/j.jpowsour.2015.03.079

[29] Agarwal, A. and B.R.J.C.E.J. Sankapal, Ultrathin Cu2P2O7 nanoflakes on stainless steel substrate for flexible symmetric all-solid-state supercapacitors. 2021. 422: p. 130131; https://doi.org/10.1016/j.cej.2021.130131

[30] Pujari, S.S., et al., Journal of Electronic Materials, 2020. 49(6): p. 3890-3901; https://doi.org/10.1007/s11664-020-08095-w